

Nature of cobalt species during the *in situ* sulfurization of Co(Ni)Mo/Al₂O₃ hydrodesulfurization catalysts

Mustafa al Samarai,^{a,†} Christa H. M. van Oversteeg,^a Mario Ulises Delgado-Jaime,^a Tsu-Chien Weng,^b Dimosthenis Sokaras,^b Boyang Liu,^a Marte van der Linden,^{a,c} Ad M. J. van der Eerden,^a Eelco T. C. Vogt,^a Bert M. Weckhuysen^a and Frank M. F. de Groot^{a,*}

Received 5 January 2019
Accepted 18 February 2019

Edited by S. M. Heald, Argonne National Laboratory, USA

[†] Present address: Max Planck Institute for Chemical Energy Conversion, Stiftstrasse 34, D-45470 Mulheim, Germany.

Keywords: heterogeneous catalysis; hydrodesulfurization (HDS) catalyst systems; CoMoS structure; hydrotreating catalysts; X-ray absorption spectroscopy; resonant inelastic X-ray scattering (RIXS).

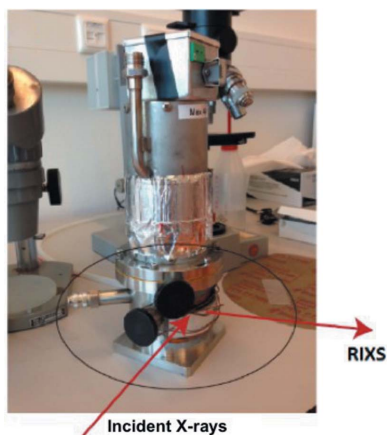
Supporting information: this article has supporting information at journals.iucr.org/s

^aInorganic Chemistry and Catalysis, Debye Institute for Nanomaterials Science, Utrecht University, Universiteitsweg 99, 3584 CG Utrecht, The Netherlands, ^bStanford Synchrotron Radiation Lightsource, SLAC National Laboratory, 2575 Sandhill Road, Menlo Park, CA 94025, USA, and ^cID26, European Synchrotron Radiation Facility (ESRF), 71 Avenue des Martyrs, 38000 Grenoble, France. *Correspondence e-mail: f.m.f.degroot@uu.nl

The evolution in local structure and electronic properties of cobalt was investigated during *in situ* sulfurization. Using a combination of 1s X-ray absorption (XAS) and 1s3p resonant inelastic X-ray scattering (RIXS), the valence, coordination and symmetry of cobalt ions were tracked in two cobalt-promoted molybdenum oxide precursors of the hydrodesulfurization catalyst system, namely Co–Mo/Al₂O₃ and Co–Ni–Mo/Al₂O₃. Extended X-ray absorption fine structure shows that the Co–O bonds were replaced with Co–S bonds as a function of reaction temperature. The cobalt *K* pre-edge intensity shows that the symmetry of cobalt was modified from Co³⁺ *O_h* and Co²⁺ *O_h* to a Co²⁺ ion where the inversion symmetry is broken, in agreement with a square-pyramidal site. The 1s3p RIXS data revealed the presence of an intermediate cobalt oxy-sulfide species. This species was not detected from XAS and was determined from the increased information obtained from the 1s3p RIXS data. The cobalt XAS and RIXS data show that nickel has a significant influence on the formation of the cobalt oxy-sulfide intermediate species prior to achieving the fully sulfided state at *T* > 400°C.

1. Introduction

The development of novel hydrodesulfurization (HDS) catalysts has been one of the interesting research subjects in the field of heterogeneous catalysis because of the new environmental regulations to reduce sulfur emissions of transportation fuels (Eijsbouts *et al.*, 2008). Cobalt- and nickel-promoted molybdenum sulfide catalysts supported on porous oxides, such as alumina, have been used since the early years of the previous century. The active phase of this catalyst is assumed to consist of MoS₂ slabs with cobalt and/or nickel decorating the edges. There are many factors that can affect the activity of a catalytic solid, *e.g.* the metal loadings, type of support and especially the synthesis conditions and treatment procedures employed (Ratnasamy *et al.*, 1980; Keely *et al.*, 1984; Topsøe, Clausen, Topsøe & Pedersen *et al.*, 1986; Topsøe & Clausen, 1986; Prins *et al.*, 1989; Breysse *et al.*, 1991; Chianelli *et al.*, 1994; Startsev, 1995). Numerous studies have attempted to explain the catalytic HDS process and describe the role of the involved promoters Co and Ni on the Al₂O₃-supported MoS_x phase. The Co–MoS_x structure originally proposed by Topsøe and co-workers and Grunwaldt *et al.* (2004) was also



OPEN ACCESS

confirmed by Bouwens *et al.* (1990, 1991, 1994) and Crajé *et al.* (1991*a,b*). The catalytic performance of this active phase is determined by the structure of the oxide precursor species, which is strictly dependent on the preparation methods (Topsøe *et al.*, 1984; Kibsgaard *et al.*, 2010). Therefore, as a starting point it is crucial to understand the processes involved in the synthesis of the catalyst and especially the sulfurization/activation step. In the petrochemical industry, the oxide precursors are activated by the addition of sulfur-containing compounds, *e.g.* methyl sulfides, to the feedstock. However, usually a mixture of 10% H₂S/H₂ is used to sulfurize the (supported) oxide precursors. Among the many synthesis steps involved, the sulfurization process is very likely the step that determines the final structure and performance of the active Co–Ni–Mo/Al₂O₃ catalyst material. Following the analysis of Topsøe and Clausen, we start from the assumption that cobalt can occur in three forms in alumina-supported catalysts: (a) as cobalt ions on the edges of the MoS₂ crystallites, (b) as Co₉S₈ particles and (c) as divalent cobalt ions at the surface or in the bulk of the alumina (Topsøe *et al.*, 1984). Several characterization studies focused on the changes in (cobalt-doped) molybdenum compounds during the sulfidation process (Scheffer *et al.*, 1984; Arnoldy *et al.*, 1985; Nicosia & Prins, 2005; Rochet *et al.*, 2016). Recently Šarić *et al.* performed detailed density functional theory calculations of the Co–MoS_x system (Šarić *et al.*, 2017, 2018). They calculated the structures of the edges, basal plane and corners of the MoS₂ slabs and found that the HDS activity is related to the small energy differences between structures with or without a sulfur atom for the corners and the S edges, but not the Mo edges.

In this article, we study the valence, coordination and spin-state changes of cobalt in single (cobalt-) and double (cobalt-nickel-) promoted HDS catalysts, using a combination of 1s X-ray absorption (XAS) and 1s3p resonant inelastic X-ray scattering (RIXS). The 1s core levels of the 3d transition metal ions can be probed with hard X-rays (4–10 keV). In contrast to the main K-edge, which arises from the dipole allowed transition of 1s to 4p, the pre-edge involves mainly 1s3d quadrupole transitions. The K pre-edge energy position and intensity are sensitive to the metal oxidation state, the site symmetry, and the crystal-field splitting. However, because of their relatively low intensity and large core hole lifetime broadening, their analysis is often limited to the energy position and intensity of the pre-edge. In a 1s3p RIXS experiment, the resonant 1s3p X-ray emission is measured by tuning the energy of the incident energy to a 1s X-ray absorption edge. This effectively combines X-ray absorption and X-ray emission into a single experiment (Glatzel *et al.*, 2009; Kotani *et al.*, 2001). The RIXS process can be viewed as an inelastic scattering of the incident photon at a resonance energy of the metal ion and is theoretically described by the Kramers–Heisenberg formula (Sakurai, 1967; Rubensson, 2000). The spectral broadening of 1s XAS is determined by the lifetime of the 1s intermediate state (L_{1s}), whereas the spectral broadening of the 1s3p resonant XES depends on the final state 3p lifetime (L_{3p}) (Glatzel *et al.*, 2005; Hill *et al.*, 1998). Because

L_{1s} is larger than L_{3p} , this results in the observation of spectral features on the X-ray emission energy scale with sharper line width than in a conventional X-ray absorption spectrum.

Hard X-rays are able to penetrate solids and probe the bulk phase properties of the samples (van Bokhoven *et al.*, 2004; Rabe *et al.*, 2010; Szlachetko *et al.*, 2013). This allows the determination of the active sites within the bulk of the sample under *in situ* conditions. In this work, RIXS is used to study the composition of the Co–Mo/Al₂O₃ and Co–Ni–Mo/Al₂O₃ HDS catalysts as model systems to reflect the abilities of the RIXS technique to study other heterogeneous catalysts under *in situ* conditions. The purpose of the present work is to unravel the nature of the cobalt species in the precursor oxide of γ -Al₂O₃-supported Co–Mo and Co–Ni–Mo catalysts and to follow the changes in the local structure and electronic properties, during the *in situ* sulfurization with RIXS and XAS.

2. Materials and methods

2.1. Sample preparation

The Co–Mo/Al₂O₃ and Co–Ni–Mo/Al₂O₃ catalyst materials were both synthesized by incipient wetness impregnation of the γ -Al₂O₃ support (BASF Al-4184, surface area of 157 m² g⁻¹ and pore volume of 0.75 ml g⁻¹) with a solution of metal salts. Aqueous solutions of ammonium heptamolybdate hexahydrate [AHM, (NH₄)₆Mo₇O₂₄·6H₂O, Sigma Aldrich, ≥99.0%], cobalt nitrate hexahydrate [Co(NO₃)₂·6H₂O, Acros Organics, 99+ %] for Co–Mo/Al₂O₃ and additionally nickel nitrate hexahydrate [Ni(NO₃)₂·6H₂O, Sigma-Aldrich, 99.999%] for Co–Ni–Mo/Al₂O₃ were co-impregnated to obtain weight loadings of 14 wt% for molybdenum and 5 wt% for both cobalt and nickel. Subsequently, both samples were dried at 60°C for 16 h then at 120°C for 1 h. To convert the impregnated metal precursors to their respective metal oxides, the samples were calcined at 450°C for 16 h. All drying and calcination steps were performed under a (75% N₂)/(25% O₂) flow (1 ml min⁻¹). We note that the atomic Co/Mo ratio of 0.58 is higher than used in the industrial HDS catalysts. We used the increased amount of cobalt and nickel to increase the signal-to-noise of the X-ray spectroscopy experiments.

During the *in situ* sulfurization experiments both oxide precursor samples were simultaneously sulfurized by loading the samples on the same sample holder. Pellets of Co–Mo/Al₂O₃ and Co–Ni–Mo/Al₂O₃ samples were made from the respective powders and loaded on the same sample holder as is shown in Fig. 1. Subsequently, the sample holder was placed inside the heating stage of the reactor. The sample was heated to 450°C with a ramp of 10°C min⁻¹, while flowing with a 10% H₂S/H₂ mixture (1 ml min⁻¹). The samples were kept at 450°C for 5 h.

The reactor was assembled and sealed and the incident window was covered with Kapton foil to decrease the photon flux and prevent radiation damage and leakage of air into the reactor. The reactor includes connections for both gas inlet and gas outlet. The inlet line is connected with a mass-flow

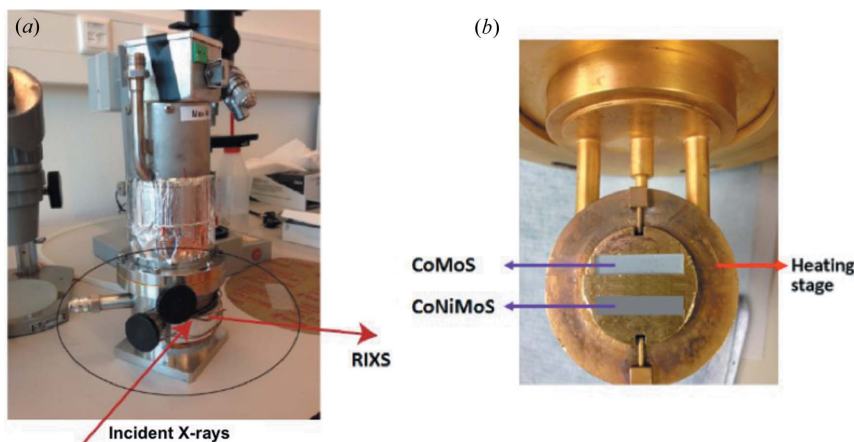


Figure 1

(a) Schematic of the dedicated sealed RIXS reactor showing the position of the incident X-rays and the scattered photons. The incident window was sealed with Kapton foil. The reactor has gas inlet (connected to a mass-flow controller) and outlet (to an exhaust stream) connections. Furthermore, to regulate the temperature the upper part of the reactor is connected to the temperature controller. (b) Overview of the sample holder with the sample pellets in the middle. The holder is placed in the heating stage.

controller that regulates the type and amount of gas that passes through the reactor. On the outlet side, there are bubbler airlocks that can be used to trap the toxic gas mixture. First, the oxide precursors were measured under ambient conditions, followed by *in situ* sulfurization under dynamic flow of 10% $\text{H}_2\text{S}/\text{H}_2$ gas mixture and by slowly heating the samples to 450°C.

2.2. X-ray experiments

The spectra were recorded at beamline 6-2 of the Stanford Synchrotron Radiation Lightsource (SSRL) (Sokaras *et al.* 2013). The beamline is equipped with two double-crystal monochromators, Si(111) and Si(311). A collimating and a focusing Rh-coated mirror are positioned before and after the monochromator, respectively. The incident energy was selected using the Si(311) crystal during the measurements at the Co K -edge. After the monochromator, the beam is delivered to the Rh-coated focusing mirror and focused both horizontally and vertically to $\sim 140 \mu\text{m} \times 400 \mu\text{m}$ ($V \times H$) at the sample position. XAS spectra were measured simultaneously in total fluorescence yield (TFY) mode using a photodiode. The sample, crystal analyzer and photon detector were arranged in a vertical Rowland geometry. The Co $K\beta$ ($1s3p$) RIXS spectra were recorded at a scattering angle of 90° in the horizontal plane using seven analyzer crystals (Bergmann & Cramer, 1998). The total energy resolution ($\Delta E/E$) of the beamline and the spectrometer is ~ 0.2 eV. The intensity was normalized to the incident flux. The RIXS data are shown as a contour map in a plane of incident and transferred photon energies, where the vertical axis represents the energy difference between the incident and emitted energies (energy-loss). The variations in colour on the plot correspond to the different scattering intensities.

The RIXS 2D maps were recorded in the excitation range 7704–7715 eV with steps of 0.2 eV, and 55 to 82 eV for the

RIXS energy loss, with steps of 0.25 eV. The TFY XAS was also recorded with a photodiode. Radiation-damage studies were performed at ambient conditions by measuring four XAS spectra to check for any shifts in the edge jump energy, and the pre-edge intensity and its energy shift. Additionally, RIXS spectra were measured to reconfirm the results obtained with XAS. For all spectra, there was no change in the measured spectra for a 3 h experiment, confirming the absence of radiation damage.

3. Results

3.1. Catalytic activity testing

Before presenting the results of the *in situ* sulfurization, we briefly discuss the catalytic activity of the Co–Mo–S/ Al_2O_3 and Co–Ni–Mo–S/ Al_2O_3 catalysts towards the thiophene desulfurization. The HDS reaction of thiophene was performed using thiophene saturated H_2 flow in a single-pass tubular down-flow fixed-bed reactor at the reaction conditions of 320°C. Fig. 2 shows a schematic summary of the performed catalytic studies. Prior to the reaction, the catalyst was reduced and sulfided for 6 h at 450°C at a heating rate of 5°C min^{-1} under a gas mixture containing 10 mol% H_2S in H_2 and a flow rate of 1 ml min^{-1} . The initial activity test (the first pulse) was performed under 0.1 μl of thiophene saturated in 10 ml min^{-1} H_2 , at a temperature of 320°C. The sample was then stabilized using 1 μl thiophene saturated H_2 with a flow rate of 10 ml min^{-1} at 320°C. Following a stabilization step, the catalytic activity of the samples was measured under similar conditions. The gaseous products were analyzed online on a mass spectrometer through a sampling and a flame ionization detector. Fig. 3 shows the normalized conversions of thiophene by Co–Ni–Mo–S/ Al_2O_3 and Co–Mo–S/ Al_2O_3 during three subsequent HDS steps. Since variation in molybdenum-loading influences the HDS activity, the conversion is normalized for the molybdenum loading of the catalysts. An initial conversion of 27% was observed for the double promoted catalyst and 60% for the single promoted catalyst material. The thiophene conversion data were normalized to the Mo loading.

Because of the higher ratio of promoters to molybdenum in Co–Ni–Mo–S/ Al_2O_3 , an increase in the formation of bulk cobalt- and nickel sulfide phases is expected, resulting in a reduced catalytic activity. The lower conversions observed for Co–Ni–Mo–S/ Al_2O_3 can be explained by a decrease in the number of promoter atoms on the edges of MoS_2 slabs. In addition, as shown in Fig. 3, an increase in the conversion rate was observed for the subsequent thiophene pulses. This increase is caused by the correlation between the dispersion, degree of sulfidation of active phase and the HDS activity. Note that, because of the thiophene treatment steps, the

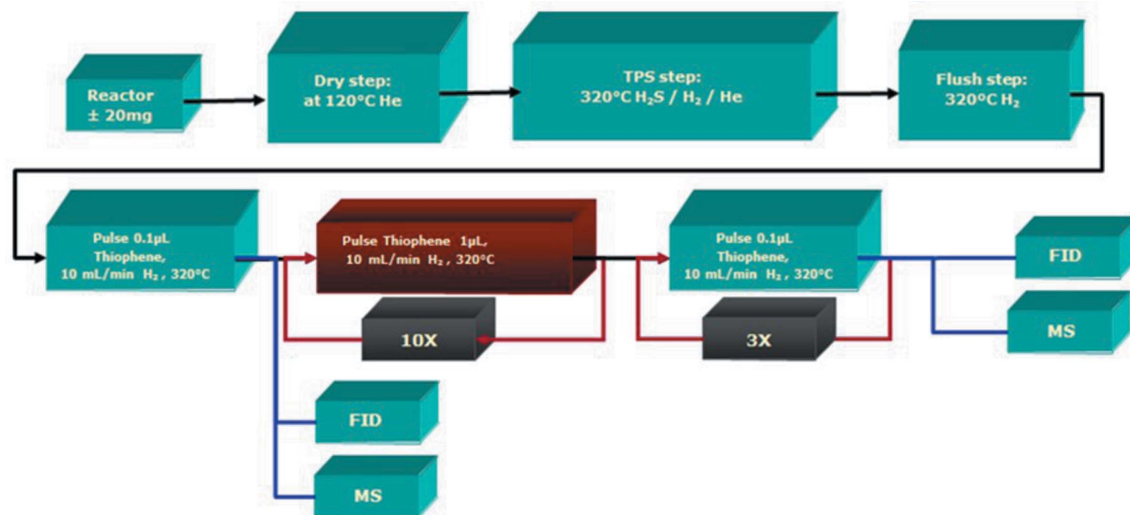


Figure 2 Schematic presentation showing the conditions used during catalytic thiophene desulfurization activity tests of the freshly sulfided Co–Mo–S/Al₂O₃ and Co–Ni–Mo–S/Al₂O₃ catalyst material, during subsequent steps of the thiophene HDS reaction.

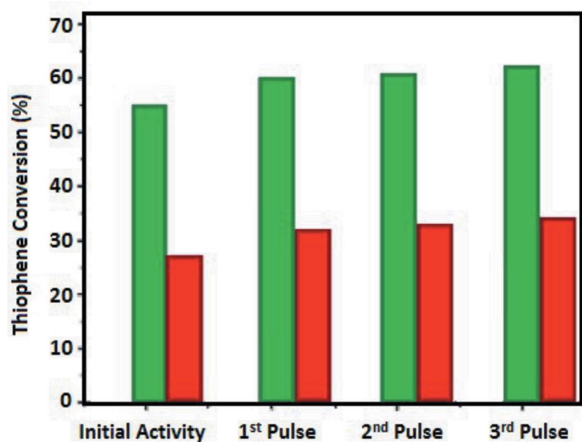


Figure 3 The normalized conversion of thiophene by the Co–Mo–S/Al₂O₃ (green) and Co–Ni–Mo–S/Al₂O₃ (red) catalyst materials during three different desulfurization steps. For these catalytic tests (10%) thiophene-saturated H₂ flow was used.

degree of sulfidation and dispersion of the active phase is increased.

3.2. XANES and EXAFS analysis

The X-ray absorption spectra were normalized according to the procedure described in the supporting information. Fig. 4 shows the normalized cobalt *K*-edge X-ray absorption near-edge (XANES) region as a function of temperature. The cobalt *K*-edge spectrum of freshly calcined Co–Mo/Al₂O₃ is characterized by an intense main edge (*1s* → *4p*) and a weak pre-edge feature with a main peak at 7709 eV followed by a weak shoulder at 7711.4 eV. This finding is similar to the previously reported Co₃O₄ reference (al Samarai *et al.*, 2016). Exposing both samples to the gas mixture at room temperature results in a significant shift of the main edge to lower energies implying a partial reduction of cobalt species accompanied by a decrease in the intensity of the pre-edge

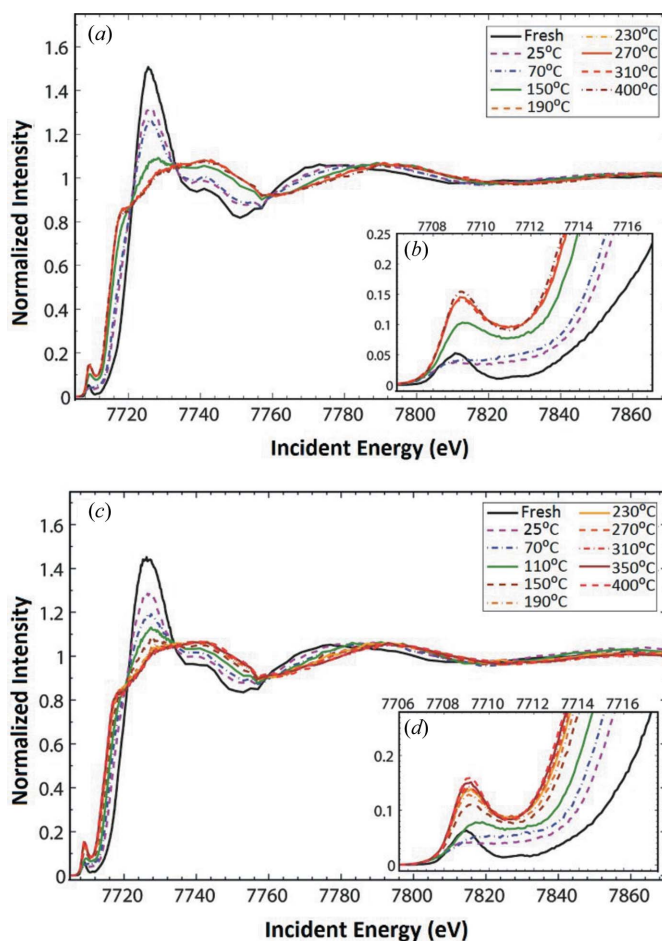


Figure 4 (a) Normalized Co *K*-edge XANES spectra for the Co–Mo/Al₂O₃ catalyst at various reaction temperatures and under an atmosphere of 10% H₂S/H₂; (b) inset of (a) around the pre-edge region. (c) Normalized Co *K*-edge XANES spectra for the Co–Ni–Mo/Al₂O₃ catalyst at various reaction temperatures and under an atmosphere of 10% H₂S/H₂; (d) inset of (c) around the pre-edge region.

feature. In addition, the pre-edge intensity grows dramatically and the spectral shape is modified for both catalysts.

Upon heating the catalysts to higher reaction temperatures, the main edge shifts to lower energies, indicating a further reduction. In Fig. 5 the normalized intensity of the pre-edge of Co–Mo/Al₂O₃ and Co–Ni–Mo/Al₂O₃ shows an increase for $T < 200^\circ\text{C}$, while for $T > 200^\circ\text{C}$ the pre-edge intensity is not further increased. The details of the fits including all numbers are given in Tables S2 and S3 of the supporting information. The increase in pre-edge intensity is assigned to a reduction in symmetry of Co³⁺ O_h and Co²⁺ O_h in the cobalt oxide species to a Co²⁺ ion in a square-pyramidal cobalt sulfide species for the fully sulfided catalyst sample (Borges *et al.*, 2012; Orita *et al.*, 2004; Paul *et al.*, 2008; Ma & Schobert, 2000). In this case, the crystal field splits the 3*d* orbitals partly belonging to the same irreducible representation of the point group as metal 4*p* orbitals, leading to partial mixing and hybridization (Griffith, 1964; Figgis, 1966). The increase in the pre-edge intensity is ascribed to the increase in the degree of the 3*d*4*p* mixing/hybridization character of the orbitals. We note that the pre-edge intensity is equivalent to that found in other studies (Nicosia & Prins, 2005; Rochet *et al.*, 2016) and lower than the pre-edge in Co₉S₈, which contains 50% tetrahedral and 50% octahedral sites. The observed pre-edge intensity indicates that if tetrahedral sites exist they relate to a maximum of 25% of the cobalt sites, the other 75% being octahedral.

In the performed composition analysis (listed in Tables S2 and S3), the Co–Mo/Al₂O₃ sample shows a higher rate of sulfidation compared with the Co–Ni–Mo/Al₂O₃ sample (Fig. 8). The Co–Mo/Al₂O₃ sample shows the complete sulfidation at 190°C, whereas the Co–Ni–Mo/Al₂O₃ sample is only fully sulfided at 400°C. Furthermore, these results are confirmed by the increase in the integrated pre-edge intensities and the analysis of the extended X-ray absorption fine structure (EXAFS) region during the sulfuration process, which was sensitive to mainly the presence of either Co–O or Co–S bonds. The EXAFS analysis illustrates the considerable impact that the temperature has on the sulfuration process and on the formation of Co–S bonds under the flow of the 10% H₂S/H₂ gas mixture (Fig. S6). At room temperature, approximately 45% and 50% of the total bonds are converted to Co–S bonds for Co–Mo/Al₂O₃ and Co–Ni–Mo/Al₂O₃ samples, respectively. This increase is attributed to gradual ligand substitution and conversion of cobalt ions at O_h sites in

the case of the oxide precursor to the (C_{4v}) square-pyramidal cobalt in symmetry for the fully sulfided sample.

3.3. 1*s*3*p* RIXS analysis

A series of cobalt 1*s*3*p* RIXS planes were recorded during the *in situ* sulfuration of Co–Mo/Al₂O₃ and Co–Ni–Mo/Al₂O₃. Fig. 6 shows the temperature-dependent 1*s*3*p* RIXS spectra of Co–Mo/Al₂O₃. The equivalent 1*s*3*p* RIXS spectra of Co–Ni–Mo/Al₂O₃ are shown in Section S3. The figure shows several changes during the *in situ* sulfuration reaction, including (a) the gradual conversion of two distinct pre-edge features to a single emission feature and (b) a shift of the main edge to lower absorption energies.

For every RIXS plane the emission slice at the pre-edge peak position of 7709 eV was measured as shown in Fig. 7. The equivalent graphs of the Co–Ni–Mo/Al₂O₃ catalyst are shown in Figs. S4 and S5. The oxide precursor has distinctive resonance peaks at 7650.7 eV (peak 1) and 7647.45 eV (peak 2) characteristic of divalent cobalt species (al Samarai *et al.*, 2016). Subsequently, in the following steps, as the sample was exposed to the gas mixture, the RIXS spectra were affected and the resonant emission intensity ratios of the two peaks were reversed with peak 1 at 7648.15 eV and peak 2 at 7650.65 eV. This change can be ascribed to partial sulfidation of cobalt oxide species leading to modification in the symmetry of Co²⁺ ions.

The RIXS spectra were fit according to a procedure that involved a linear combination of the RIXS data on the freshly calcined sample (assumed to be in its oxide form) and the sample at 400°C for each temperature in addition to a small offset value to account for the counts on the tails of other emission processes. Initially, to fit the RIXS data, the combination of only two components was used to analyse the spectra. However, this proved to be impossible as additional peaks were observed in the experimental spectra during the *in situ* reaction. Therefore, additional empirical peaks were added to the model and collectively denoted as ‘intermediate species’. However, we imposed an important constraint to these empirical peaks: the broadening, shape energy position and relative intensities were forced to be the same in all spectral series (for all temperatures) by holistically fitting all spectra. We performed 100 fits in each stage of the *in situ* reaction using the methodology implemented in *Blueprint*

XAS to explore uncertainty of all fit parameters (Delgado-Jaime *et al.*, 2010; Delgado-Jaime & Kennepohl, 2010). We then selected the best fits on the basis of the lowest sum squared error (SSE).

3.4. Combined analysis of XANES, EXAFS and RIXS

The obtained phase concentrations are shown in Fig. 8. In the case of the Co–Mo/Al₂O₃ sample the RIXS data

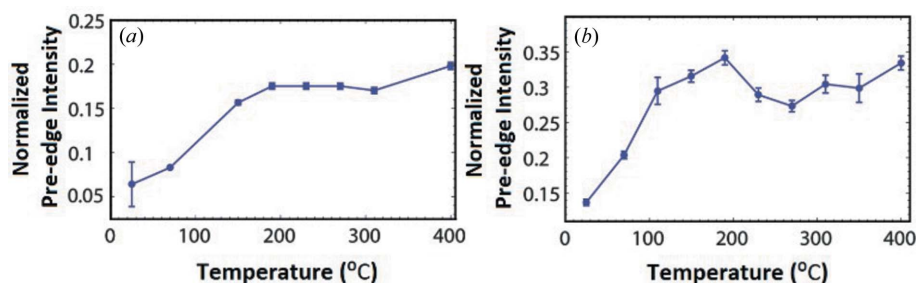
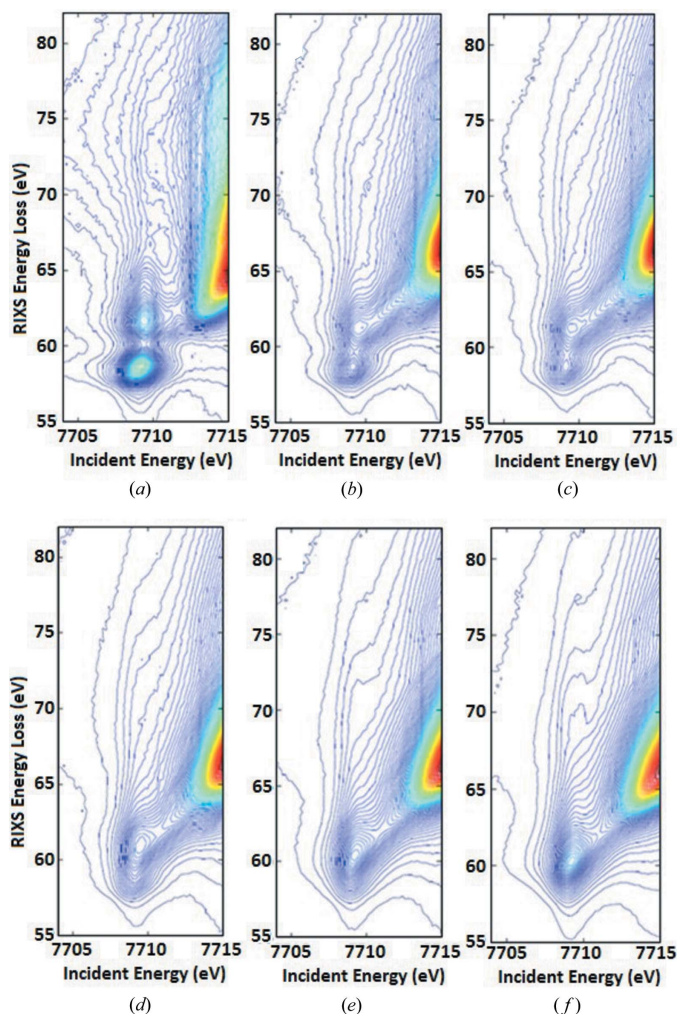


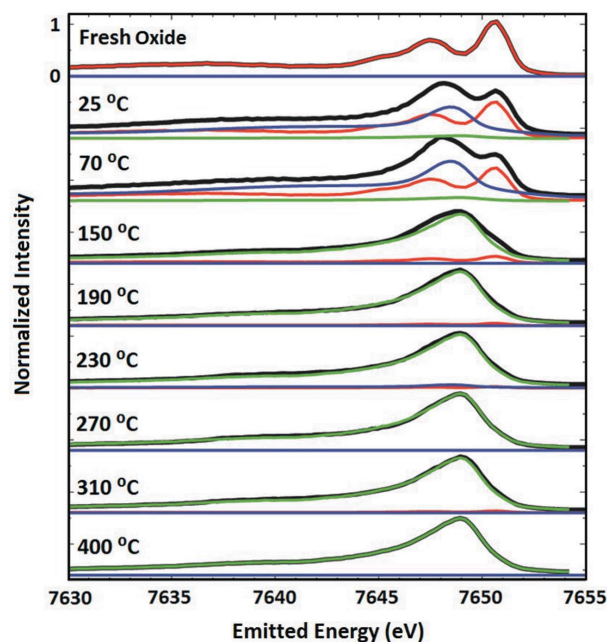
Figure 5
Pre-edge intensity areas of the Co K-edge XANES spectra of the (a) Co–Mo/Al₂O₃ and (b) Co–Ni–Mo/Al₂O₃ catalyst as a function of reaction temperature. If no error bars are given they are too small to be visible.


Figure 6

The experimental Co $1s3p$ RIXS data of Co–Mo/Al₂O₃. The freshly calcined sample was measured at 25°C (a). Subsequently we used gradual sulfidation by heating the sample under a dynamic 10% H₂S/H₂ gas mixture flow to 25°C (b), 70°C (c), 110°C (d), 150°C (e), and 400°C (f).

analysis revealed the presence of a single intermediate species (in blue) for the lower temperatures ($T < 150^\circ\text{C}$). Because of its spectral shape, we can assume a species consisting mostly of Co–S bonds. However, the fitting of the Co–Ni–Mo/Al₂O₃ RIXS data was only possible by the inclusion of two intermediate species (blue and purple), which remain present during the *in situ* reaction for $T < 400^\circ\text{C}$. The shape of one of the species has a predominantly oxide character [blue in (a)], while the second has a rather sulfide character [purple in (b)]. This assumption is based upon their comparison with the spectra of the pure oxide and the pure sulfide with regard to their individual shape as well as the position and intensity of the spectral features. In other words, in Co–Mo/Al₂O₃ the intermediate is most likely to be the Co–S₅O and/or Co–S₄O₂ oxy-sulfide, which can be distinguished from Co–S₆ in some intermediate stages. In Co–Ni–Mo/Al₂O₃ we see both the Co–S₅O and/or Co–S₄O₂ oxy-sulfide (blue) and also the Co–S₁O₅ and Co–S₂O₄ oxy-sulfides (purple).

The Co–Ni–Mo/Al₂O₃ sample is more sensitive toward sulfidation at room temperature as 60% (versus 30% for Co–


Figure 7

Resonant X-ray emission spectra (black) Co–Mo/Al₂O₃ obtained as a vertical cross-section through the pre-edge maximum (7709 eV) in Fig. 6. The character of the freshly calcined oxide sample is identified as 100% oxide (red) while the sulfided sample at 400°C shows a 100% sulfided character (green). The spectrum of the intermediate species is also included in the figure (blue).

Mo/Al₂O₃) of the oxide species is already converted to either the sulfide or intermediate species under the dynamic flow of the gas mixture at 25°C. The details of the analysis and all numbers are given in Tables S4 and S5. We note that at 400°C oxidic cobalt is no longer detected, implying the absence of divalent cobalt ions in the alumina. In addition, a fraction of the sulfide phase could exist as Co₉S₈ particles.

4. Discussion

During the gradual sulfurization of cobalt in the Co–Mo/Al₂O₃ and Co–Ni–Mo/Al₂O₃ samples, an increase in the pre-edge intensity was observed. The increase is caused by the conversion of cobalt species to a species without inversion symmetry, for example in square-pyramidal symmetry. Furthermore, because of the sulfurization process the cobalt was reduced and the Co K main edge was also shifted to lower absorption energies. The EXAFS data analysis showed the gradual ligand exchange during the process of sulfurization. The relative concentration percentages of Co–O and Co–S bonds were determined by fitting the EXAFS data as the linear combination of components at the two extremes. The analysis showed a higher tendency towards sulfurization of cobalt in the case of Co–Mo/Al₂O₃. In addition, the gradual change in the composition was obtained for the subsequent steps of the *in situ* reaction.

The Co $1s3p$ RIXS study has shown a gradual transition of the cobalt oxide in the active phase to the fully sulfided species. One of the findings is that the Co–Mo/Al₂O₃ catalyst has a higher tendency for the sulfurization reaction and

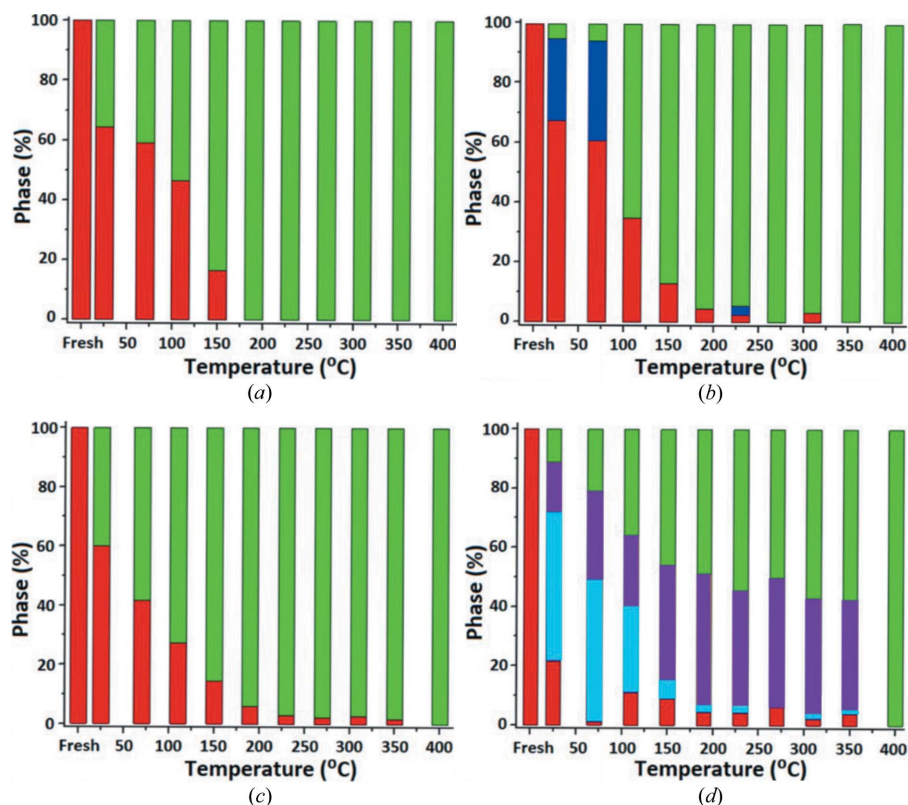


Figure 8

The phase conversion of cobalt species during the *in situ* sulfurization of Co–Mo/Al₂O₃ obtained by XANES (a) and RIXS (b). The Co–Ni–Mo/Al₂O₃ phase analysis by XANES (c) and RIXS (d) shows the presence of stable intermediates until the fully sulfided phase is obtained. In this figure, the oxide phase is indicated in red, while the fully sulfided phase is shown in green. The collection of intermediate cobalt oxysulfide species are indicated by the blue and purple.

achieves a >90% conversion to the sulfide phase at 190°C, compared with 400°C for the Co–Ni–Mo/Al₂O₃ catalyst. By analyzing the fits obtained from the RIXS data, the existence of a single intermediate species for $T \leq 150^\circ\text{C}$ with a sulfide-like character was detected for the Co–Mo/Al₂O₃ catalyst. In the case of the Co–Ni–Mo/Al₂O₃ catalyst two intermediates were identified that eventually converted to the fully sulfided

O bonds are replaced with Co–S bonds as a function of reaction temperature, and the pre-edge intensity shows that the symmetry of cobalt is modified from Co³⁺ O_h and Co²⁺ O_h to a Co²⁺ ion where the inversion symmetry is broken, in agreement with a square-pyramidal site. The cobalt 1s3p RIXS reveals the presence of an intermediate cobalt oxy-sulfide species.

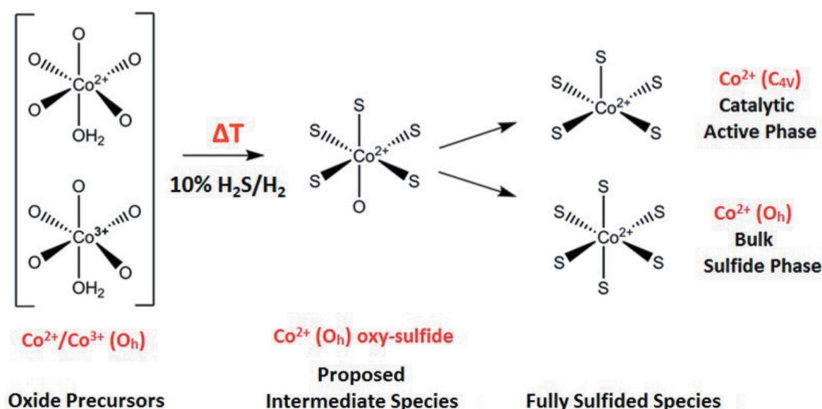


Figure 9

Representation of the proposed species involved during the *in situ* sulfurization of the freshly calcined Co–Mo/Al₂O₃ and Co–Ni–Mo/Al₂O₃. The oxide precursor was identified as octahedral Co²⁺ and Co³⁺. Prior to the complete sulfided state, cobalt oxy-sulfide intermediate species are formed. At 400°C there are two possible reaction pathways that result in either the catalytic active Co²⁺ (C_{4v}) sulfide species or the bulk Co²⁺ (O_h) sulfide species.

phase at 400°C. The RIXS data confirmed the previously obtained results by XANES and EXAFS analysis of the two samples. A summary of the proposed cobalt species involved during the *in situ* sulfurization of the Co–Mo/Al₂O₃ and Co–Ni–Mo/Al₂O₃ HDS catalysts is shown in Fig. 9. The two phases found in the fully sulfided phase are not in agreement with the recent studies of Šarić *et al.* (2017, 2018), who calculate the HDS activity as a difference between tetrahedral cobalt sites. As discussed in Section 3.2, the observed pre-edge intensity indicates that if tetrahedral sites exist they can relate to a maximum of 25% of the cobalt sites, the other 75% being octahedral. The results are in agreement with the alternative of the cobalt having square-pyramidal symmetry.

5. Conclusions

We conclude that from a combination of cobalt 1s XANES, EXAFS and 1s3p RIXS we derived several boundary conditions regarding the mechanisms of sulfurization in Co–Ni–Mo/Al₂O₃ catalysts. EXAFS shows that the Co–

The catalytic data shows a large influence of nickel in the Co–Ni–Mo/Al₂O₃ catalyst in comparison with Co–Mo/Al₂O₃. The cobalt XAS and RIXS data show that nickel has a significant influence on the formation of the cobalt oxy-sulfide intermediate species prior to achieving the fully sulfided state.

6. Supporting information

The supporting information is available as a PDF file containing information on (1) the catalytic activity testing, (2) the XAS data analysis method, (3) the numerical XANES fit results and (4) the 1s3p RIXS images of the CoNiMo catalyst.

Acknowledgements

The experiments were performed under the approvals of the Stanford Synchrotron Radiation Light source (Proposal No. 4107).

Funding information

This research is performed with financial support from STW-NWO (Netherlands Organization for Scientific Research with grant number NANO-11507).

References

- Arnoldy, P., van den Heijkant, J. A. M., de Bok, G. D. & Moulijn, J. A., (1985). *J. Catal.* **92**, 35–55.
- Bokhoven, J. A. van, Ressler, T., de Groot, F. M. F., Knop-Gericke, A. (2004). In *In-situ Spectroscopy of Catalysts*, edited by B. M. Weckhuysen. Stevenson Ranch: American Scientific Publishers.
- Bergmann, U. & Cramer, S. P. (1998). *Proc. SPIE*, **3448**, 198–209.
- Borges, I. Jr & Silva, A. M. (2012). *J. Braz. Chem. Soc.* **23**, 1789–1799.
- Bouwens, S. M. A. M., Prins, R., De Beer, V. H. J. & Koningsberger, D. C. (1990). *J. Phys. Chem.* **94**, 3711–3718.
- Bouwens, S. M. A. M., Van Veen, J. A. R., Koningsberger, D. C., De Beer, V. H. J. & Prins, R. (1991). *J. Phys. Chem.* **95**, 123–134.
- Bouwens, S. M. A. M., van Zon, F. B. M., van Dijk, M. P., van der Kraan, A. M., de Beer, V. H. J., van Veen, J. A. R. & Koningsberger, D. C. (1994). *J. Catal.* **146**, 375–395.
- Breyse, M., Portefaix, J. L. & Vrinat, M. (1991). *Catal. Today*, **10**, 489–505.
- Chianelli, R. R., Daage, M. & Ledoux, M. (1994). *J. Adv. Catal.* **40**, 177–232.
- Craje, M. W. J., de Beer, V. H. J. & van der Kraan, A. M. (1991a). *Appl. Catal.* **70**, L7–L13.
- Craje, M. W. J., De Beer, V. H. J. & van Der Kraan, A. M. (1991b). *Bull. Soc. Chim. Belg.* **100**, 953–960.
- Delgado-Jaime, M. U. & Kennepohl, P. (2010). *J. Synchrotron Rad.* **17**, 119–128.
- Delgado-Jaime, M. U., Mewis, C. P. & Kennepohl, P. (2010). *J. Synchrotron Rad.* **17**, 132–137.
- Eijsbouts, S., Battiston, A. A. & Vanleerdam, G. (2008). *Catal. Today*, **130**, 361–373.
- Figgis, B. N. (1966). *Introduction to Ligand Fields*. New York: Interscience Publishers.
- Glatzel, P. & Bergmann, U. (2005). *Coord. Chem. Rev.* **249**, 65–95.
- Glatzel, P., Sikora, M., Smolentsev, G. & Fernández-García, M. (2009). *Catal. Today*, **145**, 294–299.
- Griffith, J. S. (1964). *The Theory of Transition-Metal Ions*. Cambridge University Press.
- Grunwaldt, J. D., Caravati, M., Hannemann, S. & Baiker, A. (2004). *Phys. Chem. Chem. Phys.* **6**, 3037–3047.
- Hill, J. P., Kao, C. C., Caliebe, W., Matsubara, M., Kotani, A., Peng, J. L. & Greene, R. L. (1998). *Phys. Rev. Lett.* **80**, 4967–4970.
- Keely, W. M., Jerus, P., Dienes, E. K. & Hausberger, A. L. (1984). *Catal. Rev.* **26**, 485–502.
- Kibsgaard, J., Tuxen, A., Knudsen, K. G., Brorson, M., Topsøe, H., Laegsgaard, E., Lauritsen, J. V. & Besenbacher, F. J. J. (2010). *J. Catal.* **272**, 195–203.
- Kotani, A. & Shin, S. (2001). *Rev. Mod. Phys.* **73**, 203–246.
- Ma, X. L. & Schobert, H. H. (2000). *J. Mol. Catal. A Chem.* **160**, 409–427.
- Nicosia, D. & Prins, R. (2005). *J. Catal.* **231**, 259–268.
- Orita, H., Uchida, K. & Itoh, N. (2004). *Appl. Catal. Gen.* **258**, 115–120.
- Paul, J. F., Cristol, S. & Payen, E. (2008). *Catal. Today*, **130**, 139–148.
- Prins, R., De Beer, V. H. J. & Somorjai, G. A. (1989). *Catal. Rev.* **31**, 1–41.
- Rabe, S., Nachttegaal, M., Ulrich, T. & Vogel, F. (2010). *Angew. Chem. Int. Ed.* **49**, 6434–6437.
- Ratnasamy, P. & Sivasanker, S. (1980). *Catal. Rev.* **22**, 401–429.
- Rochet, A., Baubet, B., Moizan, V., Pichon, C. & Briois, V. (2016). *C. R. Chim.* **19**, 1337–1351.
- Rubensson, J. E. (2000). *J. Electron Spectrosc. Relat. Phenom.* **110–111**, 135–151.
- Sakurai, J. J. (1967). *Advanced Quantum Mechanics*. Reading: Addison-Wesley.
- Samarai, M. al, Delgado-Jaime, M. U., Ishii, H., Hiraoka, N., Tsuei, K. D., Rueff, J. P., Lassale-Kaiser, B., Weckhuysen, B. M., de Groot, F. M. F. (2016). *J. Phys. Chem. C*, **120**, 24063–24069.
- Šarić, M., Rossmeisl, J. & Moses, P. G. (2017). *Phys. Chem. Chem. Phys.* **19**, 2017–2024.
- Šarić, M., Rossmeisl, J. & Moses, P. G. (2018). *J. Catal.* **358**, 131–140.
- Scheffer, B., De Jonge, J. C., Arnoldy, P. & Moulijn, J. A. (1984). *Bull. Soc. Chim. Belg.* **93**, 751–762.
- Sokaras, D., Weng, T. C., Nordlund, D., Alonso-Mori, R., Velikov, P., Wenger, D., Garachtchenko, A., George, M., Borzenets, V., Johnson, B., Rabedeau, T. & Bergmann, U. (2013). *Rev. Sci. Instrum.* **84**, 053102.
- Startsev, A. N. (1995). *Catal. Rev.* **37**, 353–423.
- Szlachetko, J., Sá, J., Safonova, O. V., Smolentsev, G., Szlachetko, M., van Bokhoven, J. A. & Nachttegaal, M. (2013). *J. Electron Spectrosc. Relat. Phenom.* **188**, 161–165.
- Topsøe, H. & Clausen, B. S. (1986). *Appl. Catal.* **25**, 273–293.
- Topsøe, H. & Clausen, B. S. (1984). *Catal. Rev.* **26**, 395–420.
- Topsøe, H., Clausen, B. S., Topsøe, N. Y. & Pedersen, E. (1986). *Ind. Eng. Chem. Fund.* **25**, 25–36.